PROCEEDINGS of the
23rd International Congress on Acoustics

9 to 13 September 2019 in Aachen, Germany

Vibration transmission between two reinforced concrete beams with surface-to-surface contact conditions

Marios Filippoupolitis[1,2]; Carl Hopkins[1,2]

[1] Institute for Risk and Uncertainty, University of Liverpool, UK

[2] Acoustics Research Unit, University of Liverpool, UK

ABSTRACT

To detect human survivors trapped in buildings after earthquakes by using structure-borne sound it is necessary to have knowledge of vibration transmission in collapsed and fragmented reinforced-concrete buildings. In this paper, Statistical Energy Analysis (SEA) is used to model vibration transmission between two reinforced concrete beams with surface-to-surface contact conditions. Experimentally validated Finite Element Models (FEM) of two elastically connected beams were used to carry out a Monte Carlo simulation with 30 beam junctions. Coupling loss factors were determined from the FEM data using Experimental SEA (ESEA) and these were compared against theoretical models based on a lump spring connector. Results are shown for bending modes, torsional modes and the combination of all modes. For only bending or torsional waves, close agreement was achieved between FEM ESEA and the analytical model up to the frequency where half the bending or torsional wavelength equaled the longest side of the contact area. When all wave types were combined, reasonable agreement could still be achieved but only at low-frequencies.

Keywords: vibration transmission, statistical energy analysis, finite element methods

1. INTRODUCTION

Earthquakes have the highest rate of mortality among all the natural disasters. From 1970 to 2009, 36% of fatalities that have occurred due to natural disasters are due to earthquakes (1). When victims are trapped inside a collapsed building, the challenge is to detect and locate survivors within a period that will allow them to be rescued. Most documented live rescues are accomplished within the first six days (2). However, important variables affect the survivability including the structure type and void space formation, the cause of the structural collapse, the survival location in the building and the speed and sophistication of available search and rescue capabilities (3). The prediction of vibration transmission in collapsed and fragmented reinforced-concrete buildings has the potential to inform decisions about the possibility to detect trapped human survivors by using structure-borne sound propagation. This research forms part of a funded project concerning an approach to search for human survivors using structure-borne sound propagation in collapsed and fragmented structures through the development, validation and use of theoretical models.

The aim of this paper is to assess the potential to use Statistical Energy Analysis (SEA) to model vibration transmission between two reinforced concrete beams when they are stacked on top of each other (i.e. without any bond connecting the two beams) to make a surface-to-surface connection. This is carried out using numerical experiments with Finite Element Methods (FEM) to create an ensemble of beam junctions for a Monte Carlo simulation which will allow use of Experimental SEA (ESEA) to determine Coupling Loss Factors (CLFs) between the beams.

The three main aspects to investigate are (a) whether it is possible to only consider one type of wave motion (e.g. bending waves) or whether two or more types of wave motion can be considered

[1] M.Filippoupolitis@liverpool.ac.uk
[2] carl.hopkins@liverpool.ac.uk

simultaneously (e.g. bending and torsional waves), (b) the modelling of the contact condition in FEM and (c) whether analytical models based on lump spring connectors can be used to model the contact condition. The first aspect concerning the use of ESEA with multiple wave types is necessary because in a collapsed structure it is not known whether one or more wave type will be excited at the surface-to-surface connection. For coupled plates with wave conversion at the junction, Hopkins (4) previously showed that with ESEA it was not always possible to identify multiple wave types when only bending waves are excited on one plate. The second aspect is partly addressed by previous work (7) using FEM of reinforced concrete beam junctions with a surface-to-surface connection that have been experimentally validated; these results indicated that a spring can be used to model the contact condition in FEM. The latter finding provides the impetus to assess analytical models based on lump spring connectors to calculate CLFs for SEA models.

2. METHODS

2.1 Finite Element Modelling

The junctions consist of two reinforced concrete beams, SS1 and SS2. SS1 is the lower beam of the junction with 6.0 m length, 0.3 m width and 0.2 m depth. SS2 is the upper beam of the junction with 5.0 m length, 0.2 m width and 0.3 m depth. Both beams are reinforced with four longitudinal steel bars of 16 mm diameter. The transverse reinforcement of both beams consists of 8 mm diameter stirrups placed at 200 mm centres along the beams.

FEM modelling was carried out using Abaqus v6.14. The solid element C3D20R (20 nodes) and the beam element B32 (3 nodes) were selected from the element library of Abaqus (5) to model the concrete and the steel bars respectively (see Figure 1). The mesh density fulfils the requirement for at least six elements per wavelength in structural and vibroacoustic problems (6).

The beams were simply supported at both ends. The interaction between the two beams was modelled using an elastic contact in the normal direction. After model updating based on previous experimental work (7) it was found that the contact stiffness followed a log-normal distribution with a mean value equal to 7.038E08 N/m. This value was used for the elastic contact in the FEM models.

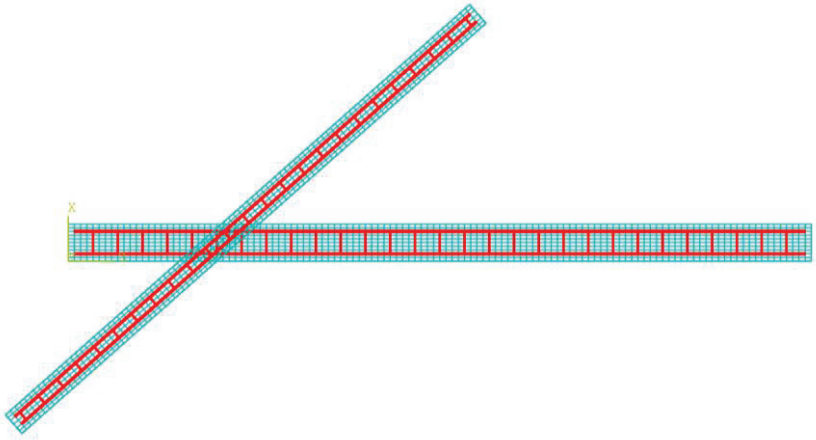

Figure 1 – Example FEM model showing the surface-to-surface connection between beams SS1 and SS2.

Table 1 shows the physical and mechanical properties of the materials used in the FEM model. The critical damping, ζ, was set to be equal to 0.05.

Table 1: Material properties

Material	Density, ρ [kg/m^3]	Young's modulus, E [N/m^2]	Poisson's ratio, ν [-]
Concrete	2287	34.7E09	0.2
Steel	7800	200E09	0.3

Mode-based steady-state dynamic analysis was used to calculate the dynamic response of the beam junctions up to 3200 Hz considering only the out-of-plane bending modes or only the torsional modes or the combination of all modes. Results are shown for 16 frequency bands with a bandwidth of 200 Hz in the frequency range from 1 to 3200 Hz.

2.2 Driving-point mobilities

Driving-point mobilities of the individual beams SS1 and SS2 were calculated with FEM using steady-state dynamic analysis at frequencies up to 3200 Hz, by using (a) only the out-of-plane bending modes, (b) only the torsional modes or (c) all modes. The upper surface of beam SS1 and the lower surface of beam SS2 were excited using a unit force (perpendicular to the surface) with random phase (i.e. rain-on-the-roof excitation) on 124 and 104 nodes respectively.

2.3 Monte Carlo simulation for ESEA

The experimentally validated FEM model was used as a basis for creating a sample of 30 beam junctions using a Monte Carlo simulation with FEM. For convenience the angle between the two beams was fixed at 41° so that the length of the longest side of the surface-to-surface contact area, $L_{C,max}$, was constant. The relative position of the two beams was defined by the coordinates of the centroid of beam SS2, $C_{SS2}(x, y)$. These were sampled from the uniform distributions $C_{SS2}(x) \sim U(-2.68, 2.68)$ and $C_{SS2}(y) \sim U(-1.43, 1.43)$ with the rule that the black shaded area in Figure 2 which indicates the surface-to-surface connection area is constant and equal to 0.091 m^2.

The beams were excited using rain-on-the-roof excitation (i.e. forces with unity magnitude and random phase); all the nodes of the lower surface were excited on beam SS1, and all nodes of the upper surface were excited on beam SS2.

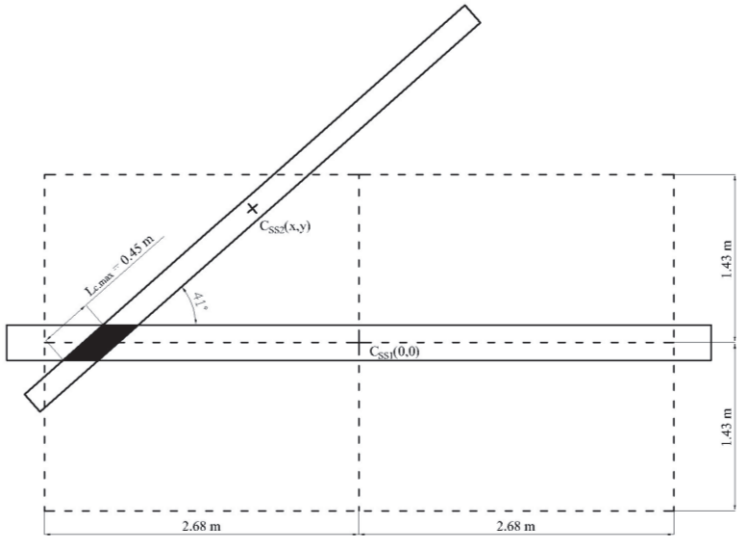

Figure 2 – Relative beam positions in the ensemble of junctions.

2.4 Experimental Statistical Energy Analysis (ESEA)

Each beam represents one subsystem and the output from the FEM models was used to calculate the subsystem energy and power input that apply to a SEA model of each beam junction. These FEM data were then used in ESEA to determine coupling loss factors.

The ESEA matrix solution for two subsystems is given by (8)

$$\begin{bmatrix} \sum_{n=1}^{2} \eta_{1n} & -\eta_{21} \\ -\eta_{12} & \sum_{n=1}^{2} \eta_{2n} \end{bmatrix} \begin{bmatrix} E_{11} & E_{12} \\ E_{21} & E_{22} \end{bmatrix} = \begin{bmatrix} \frac{W_{\mathrm{in}(1)}}{\omega} & 0 \\ 0 & \frac{W_{\mathrm{in}(2)}}{\omega} \end{bmatrix} \tag{1}$$

where η_{ij} is the coupling loss factor from subsystem i to j, η_{ii} is the internal loss factor for subsystem i and E_{ij} is the energy of subsystem i when the power is input into subsystem j, $W_{\mathrm{in}(i)}$ is the power injected into subsystem i, and ω is the angular frequency.

The energy associated with each subsystem is given by (8)

$$E = m\langle v^2 \rangle_{t,s} \tag{2}$$

where m is the mass of the subsystem and $<v^2>_{t,s}$ is the temporal and spatial average of the mean-square velocity of all the unconstrained nodes of the lower and top surfaces of subsystems SS1 and SS2 respectively.

For rain-on-the-roof excitation at P nodes, the power input, W_{in} is given by (8)

$$W_{\mathrm{in}} = \frac{\omega}{2}\sum_{p=1}^{P}\left(\mathrm{Im}\{\hat{F}\}Re\{\hat{w}\} - \mathrm{Re}\{\hat{F}\}Im\{\hat{w}\}\right)_p \tag{3}$$

where F is the force and $\hat{w}$ is the peak out-of-plane displacement associated with each node.

2.5 Analytical model based on lump spring connector

An analytical model for the surface-to-surface connection can be considered on the basis that when the wavelength of the structure-borne sound is much larger than the length of the longest edge of the surface-to-surface connection area, it can be modelled as a lump spring.

For N identical point connections between two beams, the coupling loss factor from beam i to beam j can be calculated using [e.g. see (8)]

$$\eta_{ij} = \frac{N}{\omega m_i}\frac{Re\{Y_j\}}{\left|Y_i + Y_j + Y_{\mathrm{c}}\right|^2} \tag{4}$$

where m_i is the mass of beam i, the driving-point mobility of a thin beam of infinite extent (for excitation of bending waves in the central part of the beam) is calculated using (8)

$$Y = \left((1+i)2.67\rho S\sqrt{c_{\mathrm{L,b}}hf}\right)^{-1} \tag{5}$$

and the mobility of the point connection, Y_{c}, can be calculated using (8)

$$Y_{\mathrm{c}} = \frac{i\omega}{k} \tag{6}$$

where ρ is the density of the solid beam, S is the cross-sectional area of the beam, f is frequency, h is the depth of the beam, $c_{\mathrm{L,b}}$ is the phase velocity of the beam for quasi-longitudinal waves, k is the dynamic stiffness of the point connection acting as a spring (N/m).

3. Results

3.1 Bending and torsional wavelength

To assess the potential frequency range of application for the lump spring model, the length of the longest side of the surface-to-surface contact area, $L_{\mathrm{C,max}}$, is compared with the bending and torsional wavelength. The lump spring model is expected to be valid at frequencies where $\lambda_{\mathrm{B}}/2 >> L_{\mathrm{C,max}}$ for bending motion and $\lambda_{\mathrm{T}}/2 >> L_{\mathrm{C,max}}$ for torsional motion.

Figure 3 shows the bending wavelength, λ_{B} and the half-wavelength, $\lambda_{\mathrm{B}}/2$ for beam SS1 and SS2. $L_{\mathrm{C,max}}$ is equal to $\lambda_{\mathrm{B}}/2$ for beams SS1 and SS2 at 1720 Hz and 2580 Hz respectively. For torsional waves, $L_{\mathrm{C,max}}$ is equal to $\lambda_{\mathrm{T}}/2$ for beams SS1 and SS2 at 2360 Hz.

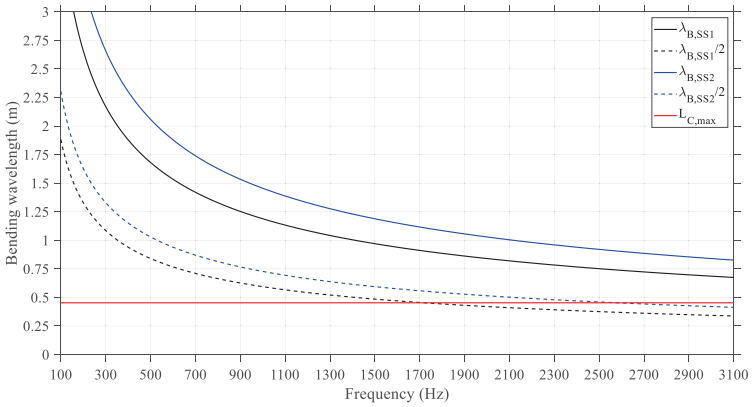

Figure 3 – Bending wavelength, λ_B of beams SS1 and SS2. The red line indicates the length of the longest side, $L_{C,max}$=0.45 m of the contact area.

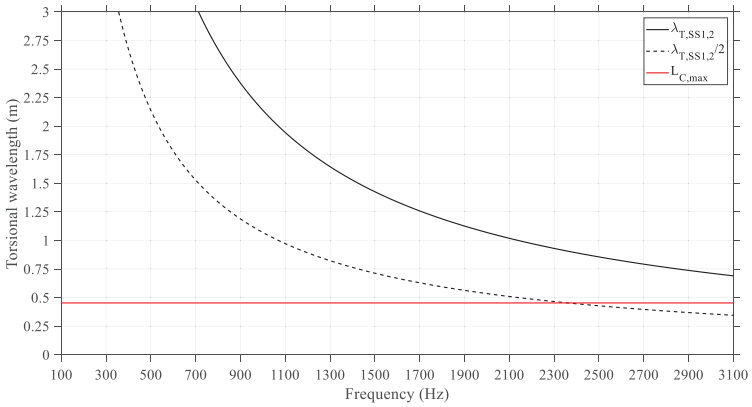

Figure 4 – Torsional wavelength, λ_T of beams SS1 and SS2. The red line indicates the length of the longest side, $L_{C,max}$=0.45 m of the contact area.

3.2 Assessment of the FEM driving-point mobilities

Figure 5 and 6 compare the spatial average of the driving-point mobilities of beams SS1 and SS2 from FEM using either bending or torsional or all modes against the driving-point mobilities of a thin beam of infinite extent for bending wave excitation (Eq. 5). Results are shown for both the real part and the magnitude that are used in Eq.(4) to calculate the CLF.

The lowest local bending mode frequency for isolated beams SS1 and SS2 is 9.7 and 21.4 Hz respectively. For bending wave excitation of beams SS1 and SS2, the ratio $Y_{B,FEM}/Y_{B,Inf}$ is below 3 dB between the 100 and 3100 Hz frequency bands, both in terms of the real part and the magnitude of the driving point mobilities.

The lowest local torsional mode frequency for isolated beams SS1 and SS2 is 164.4 and 172.8 Hz respectively. For torsional wave excitation, the ratio $Y_{T,FEM}/Y_{B,Inf}$ is below 3 dB between the 300 and 3100 Hz bands. However, in the 100 Hz band the ratio is up to 7 dB.

For all modes (i.e. the combination of bending, torsional and longitudinal modes) of beams SS1 and SS2, the ratio $Y_{A,FEM}/Y_{B,Inf}$ is below 6 dB between the 100 and 3100 Hz frequency bands, both in terms of the real part and the magnitude of the driving point mobilities.

For beam SS1 (which is thinner in the direction of bending wave motion) the infinite beam mobility is a reasonable estimate for both bending and torsional modes and whilst it is also reasonable for bending waves on SS2, it is less reasonable for torsional modes. For both beams the infinite beam theory does not give a reasonable estimate for the combination of all modes. However, due to the differences between the FEM and the infinite beam mobilities, both will be used to calculate the CLF in Section 3.3.

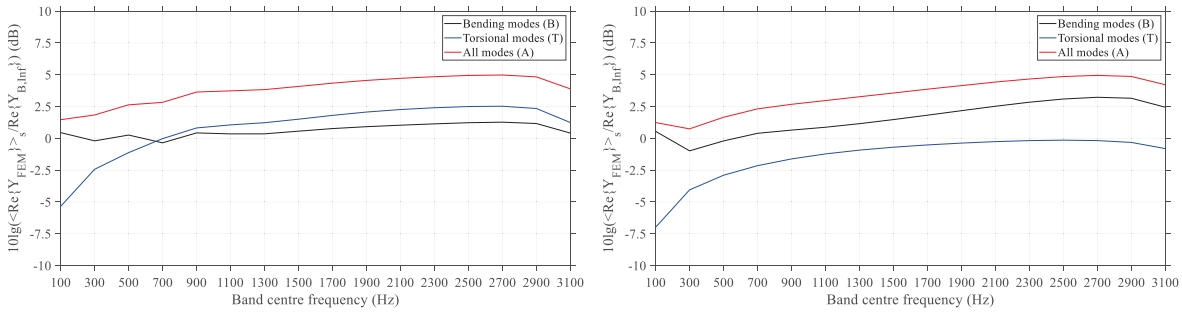

Figure 5 – Ratio of the real part of the driving-point mobilities (FEM to infinite beam theory) for beam SS1 (left) and beam SS2 (right).

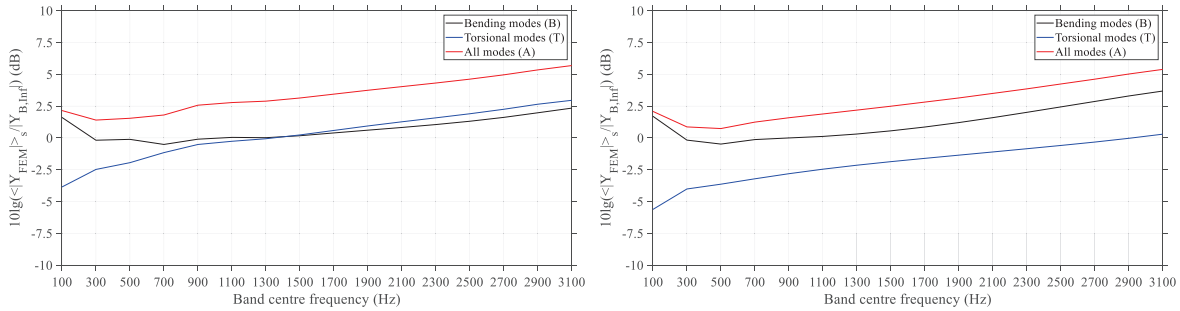

Figure 6 – Ratio of the magnitude of the driving-point mobilities (FEM to infinite beam theory) for beam SS1 (left) and beam SS2 (right).

3.3 Comparison of coupling loss factors from lump spring theory and FEM ESEA

Figure 7 to 9 show the coupling loss factors, η_{12} and η_{21} from FEM ESEA for the 30 beam junctions along with two prediction models based on the analytical lump spring model. The FEM ESEA results are shown in terms of a mean value with 95% confidence intervals. The analytical lump spring model is calculated using (a) the driving point mobilities, $Y_{B,Inf}$, of thin beams of infinite extent for excitation of bending waves in the central part of the beams and (b) the spatial average of the FEM driving point mobilities, Y_{FEM}, over the surface of beams SS1 and SS2.

For bending waves only in the FEM model (Figure 7), there is reasonable agreement between the coupling loss factors from FEM ESEA and the analytical model up to the 1700 Hz frequency band (where $\lambda_B/2 >> L_{C,max}$), with differences up to 5 dB. Above 1700 Hz, the differences increased up to 12 dB where the contact area between SS1 and SS2 cannot be considered as a point connection. Using FEM mobilities instead of the infinite beam mobilities for bending wave motion did not significantly improve the agreement.

For torsional waves only in the FEM model (Figure 8), there is reasonable agreement between FEM ESEA and the analytical model up to the 2300 Hz frequency band (where $\lambda_T/2 >> L_{C,max}$), with differences up to 5 dB. Note that in two low frequency bands (100 Hz and 300 Hz) the spread of the FEM ESEA coupling loss factors was ± 5 dB. Above 2300 Hz, the differences were between 5 and 12 dB where the contact area between SS1 and SS2 cannot be considered as a point connection. The infinite beam mobilities are intended for bending rather than torsional motion but are shown for reference. Using FEM mobilities instead of the infinite beam mobilities for torsional motion did not significantly improve the agreement.

For the combination of bending, torsional and longitudinal modes (Figure 9), reasonable agreement was achieved between the FEM ESEA and the analytical model between 100 and 900 Hz, with differences up to 5 dB. The analytical model is not expected to be valid above 1700 Hz (where $\lambda_B/2 >> L_{C,max}$) but the combination of all modes seems to reduce the frequency where reasonable agreement is obtained from 1700 to 900 Hz. The infinite beam mobilities are an approximation as they intended for bending rather than all wave motion; hence it is a coincidence that the infinite beam mobilities show better agreement than the FEM calculated mobilities with the analytical model above 1100 Hz.

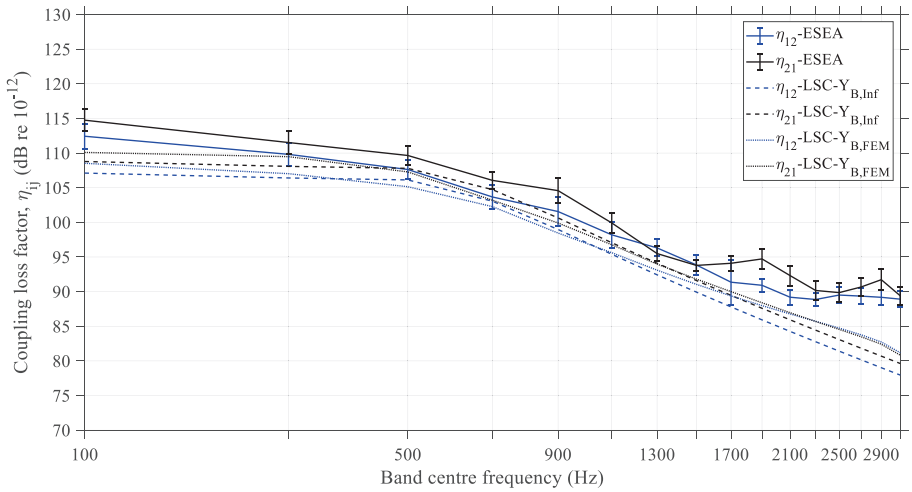

Figure 7 – Comparison of FEM ESEA (bending modes) and the analytical model (LSC) coupling loss factors η_{12} and η_{21}.

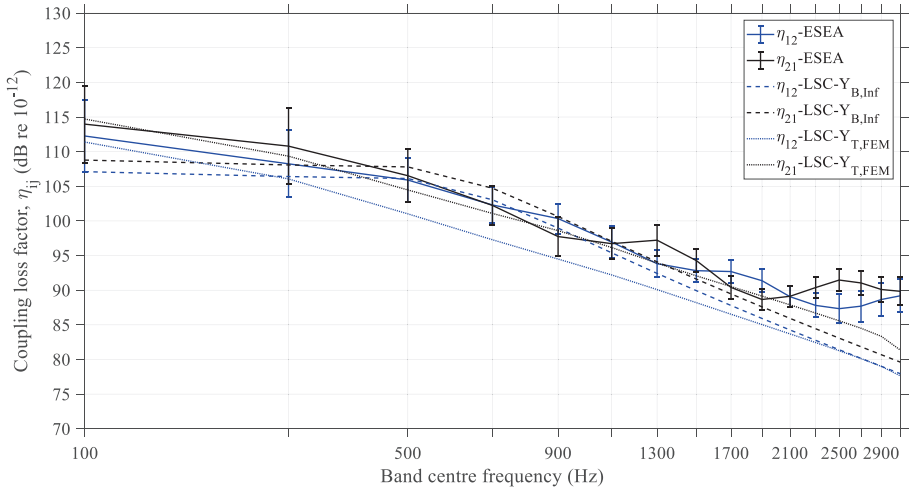

Figure 8 – Comparison of FEM (torsional modes) and the analytical model (LSC) coupling loss factors η_{12} and η_{21}.

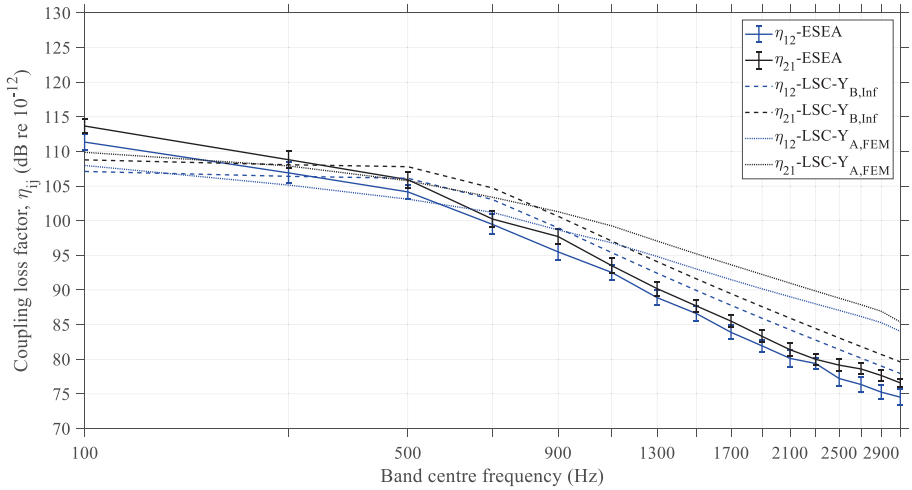

Figure 9 – Comparison of FEM (combination of all modes) and the analytical model (LSC) coupling loss factors η_{12} and η_{21}.

4. CONCLUSIONS

Finite element models were used to calculate the driving-point mobilities of reinforced concrete beams for bending modes only, torsional modes only and the combination of all modes in the frequency range up to 3200 Hz. These mobilities were in reasonable agreement with the theoretical driving-point mobilities of a thin beam of infinite extent for bending wave excitation but not for the combination of all modes.

An ensemble of 30 random beam junctions was generated for Monte Carlo simulations with FEM that allowed ESEA to be used to determine coupling loss factors between the two beams. These were compared with coupling loss factors calculated using an analytical model based on a lump spring connector. For only bending waves or torsional waves, close agreement was achieved between FEM ESEA and the analytical model up to the frequency where half the bending or torsional wavelength equaled the longest side of the contact area. Above this frequency the interaction between the two beams cannot be considered anymore as a point connection. The inclusion of the FEM driving-point mobilities in the prediction model (instead of the infinite beam model) does not significantly improve the agreement. When all wave types are combined, reasonable agreement can still be achieved at low-frequencies.

ACKNOWLEDGEMENTS

The authors are grateful for the funding provided by the EPSRC and ESRC Centre for Doctoral Training in Quantification Management of Risk & Uncertainty in Complex Systems and Environments at the University of Liverpool.

REFERENCES

1. Bobrowsky, P. T. Ed., Encyclopedia of Natural Hazards, Springer Netherlands, (2013).
2. Macintyre, A., Barbera, J. A. and Smith, E. R. Surviving Collapsed Structure Entrapment after Earthquakes: A “Time-to-Rescue” Analysis, Prehospital and Disaster Medicine, 21 (1), 4–19, (2006).
3. Macintyre, A., Barbera, J. A. and Petinaux, B. P. Survival Interval in Earthquake Entrapments: Research Findings Reinforced During the 2010 Haiti Earthquake Response, Disaster Medicine and Public Health Preparedness, 5 (1), 13–22, (2011).
4. Hopkins, C. Experimental statistical energy analysis of coupled plates with wave conversion at the junction. Journal of Sound and Vibration 2009;322:155-166.
5. Hibbitt, D., Karlsson, B. and Sorensen, P., Abaqus 6.14 Documentation and User Manual, Dessault Systemes Simulia Corp, Providence, Rhode Island (2014).
6. Atalla, N. and Sgard, F., Finite Element and Boundary Methods on Structural Acoustics and Vibration, CRC Press, Taylor & Francis Group, Boca Raton (2015).
7. Filippoupolitis, M., Hopkins, C. Investigation of support conditions between stacked reinforced concrete beams using experimental modal analysis and finite element methods, Proceedings of the 9th International Congress on Computational Mechanics, Chania, Greece, 4–6 June, (2018).
8. Hopkins, C., Sound Insulation, Butterworth-Heinemann, Oxford (2007).